Available online at www.sciencedirect.com

ScienceDirect

Mendeleev Commun., 2024, **34**, 660–663

Mendeleev Communications

Key features of perovskite solar cells *operando* stabilization with ionic liquid choline cinnamate

Elizaveta M. Nemygina,[a] Natalia N. Udalova,[a] Ekaterina I. Marchenko,[a,b] Alexandra K. Moskalenko,[a] Eugene A. Goodilin[a,c] and Alexey B. Tarasov*[a,c]

[a] *Department of Materials Science, M. V. Lomonosov Moscow State University, 119991 Moscow, Russian Federation. E-mail: alexey.bor.tarasov@yandex.ru*
[b] *Department of Geology, M. V. Lomonosov Moscow State University, 119991 Moscow, Russian Federation*
[c] *Department of Chemistry, M. V. Lomonosov Moscow State University, 119991 Moscow, Russian Federation*

DOI: 10.1016/j.mencom.2024.09.011

The ionic liquid choline cinnamate was applied for the first time as a defect passivator in light-absorbing layers of perovskite solar cells (PSCs). It was found that bulk passivation with an addition of 0.5% ionic liquid notably enhances the photothermal stability of PSCs, while surface passivation leads to the opposite effect with the loss of device stability, due to the complex origin of the influence of choline cinnamate on the defect structure and microstructure of hybrid halide perovskites.

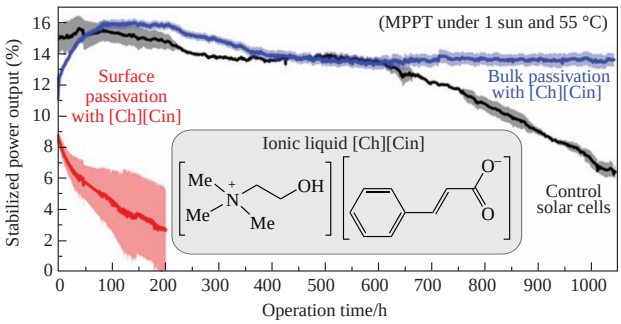

Keywords: perovskite solar cells, hybrid halide perovskites, choline cinnamate, operational stability, defect passivation, ionic liquids.

Perovskite solar cells (PSCs) are a very promising type of photovoltaic devices due to their low production costs[1,2] and record high, more than 26%, power conversion efficiency (PCE).[3] However, one of the main obstacles to their commercialization is the low operational stability of hybrid perovskites.[4–8] Although some of the negative external factors such as humidity and oxidation can be mitigated by encapsulating the entire device,[9] exposure to light and heat are unavoidable conditions inherent in solar cells operation. It is the high concentration of defects in perovskite films that triggers the degradation of the light-harvesting material, which reduces the efficiency and stability of PSCs.[10,11] Modification of perovskite materials with various organic and inorganic compounds is a widely used approach to reduce the concentration of defects in the bulk of the perovskite and at the interfaces with other layers.[12,13] Notably, there are still several emerging issues: which method of introducing a passivator, into the bulk of the perovskite or onto the surface, is more effective and what type of passivator should be optimally chosen. The use of ionic liquids (ILs) has already demonstrated a positive effect on the efficiency and stability of PSCs.[14–16] The key advantages of using ILs as perovskite modifiers are their nonvolatility, the presence of oppositely charged functional groups, high conductivity and thermal stability.[17] ILs have been successfully introduced into perovskite materials by both methods, as a bulk or as a surface passivator.[18,19] The chemical structures of previously used ILs are also very diverse,[20–22] which prompts additional research in this field to determine the optimal conditions for the passivation of hybrid perovskites with new ILs.

In this work, we compare the effects of bulk and surface passivation of perovskite films with the ionic liquid choline cinnamate, [Ch][Cin], on the performance and stability of perovskite materials and related devices. The carboxyl group of the cinnamate anion can saturate the undercoordinated lead atoms on the surface of the perovskite grains. Additionally, the aromatic ring can act as a hydrophobic tail of the anion, which is often used to modify hybrid perovskites to make them moisture resistant.[23] The choline cation containing two functional groups, –OH and $–NMe_3^+$, has already been successfully used as an effective interface passivator for hybrid perovskites.[24–26] The positively charged quaternary ammonium group has an affinity for organic cation vacancies, while the hydroxyl group can coordinate Pb^{2+} ions or occupy iodide vacancies.

All experiments were provided with the perovskite composition $(FA_{0.98}MA_{0.02})_{0.95}Cs_{0.05}Pb(I_{0.98}Br_{0.02})_3$ (FA is formamidinium ion, and MA is methylammonium ion), known as one of the most promising mixed-cation and mixed-anion compositions with superior efficiency and relatively high stability.[†,27] Comparative analysis of the morphology of perovskite films passivated with [Ch][Cin] reveals a strong

[†] Films of mixed-cationic and mixed-anionic perovskite with the composition $(FA_{0.98}MA_{0.02})_{0.95}Cs_{0.05}Pb(I_{0.98}Br_{0.02})_3$ were prepared from stoichiometric precursor solutions of formamidinium iodide (FAI), formamidinium bromide (FABr), methylammonium iodide (MAI), cesium iodide (CsI), lead bromide ($PbBr_2$) and lead iodide (PbI_2) with 30% excess methylammonium chloride (MACl) in a 4 : 1 (v/v) mixture of *N*,*N*-dimethylformamide and dimethyl sulfoxide by one-step spin-coating (6000 rpm, 30 s) in an inert glovebox. After waiting 5 s from the start of substrate rotation, a perovskite solution (35 μl) was poured, then after another 10 s of rotation, chlorobenzene antisolvent (100 μl) was poured onto the film. As-deposited film was annealed at 125 °C for an hour. Bulk passivation was carried out by adding 0.5–5 mol% [Ch][Cin] to

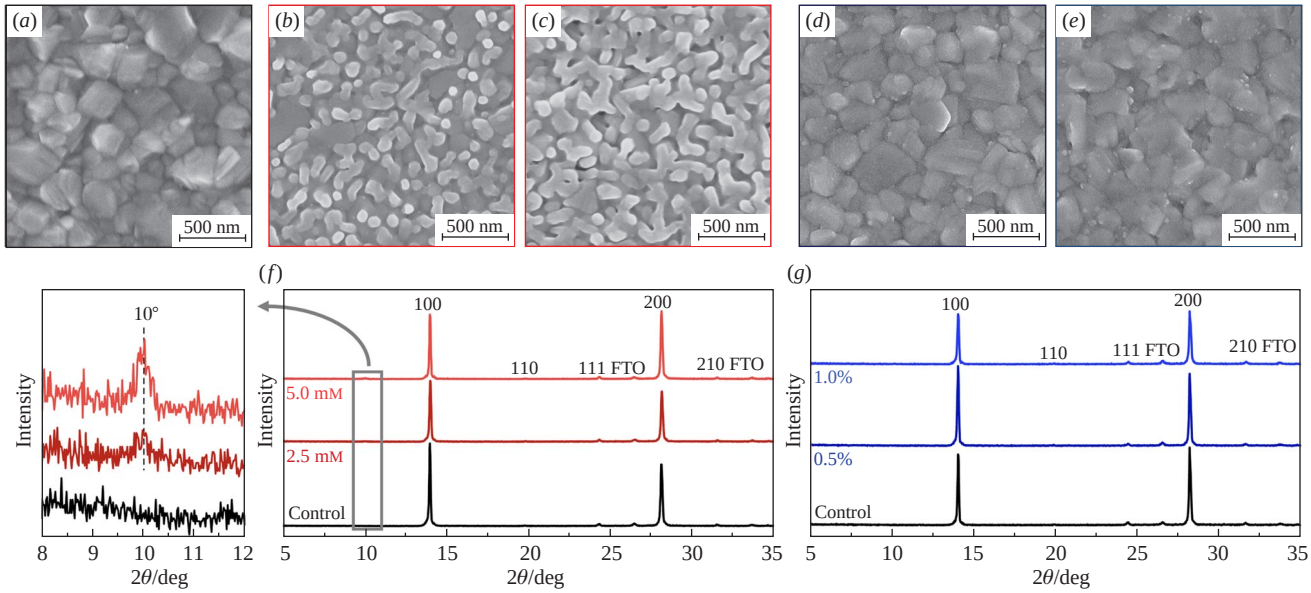

Figure 1 (*a*)–(*e*) SEM images of perovskite films: (*a*) control and passivated either on the surface with (*b*) 2.5 mM and (*c*) 5 mM IL solution, or in bulk by adding (*d*) 0.5% and (*e*) 1.0% IL to the perovskite solution. (*f*),(*g*) XRD patterns of the corresponding (*f*) surface-passivated and (*g*) bulk-passivated samples.

difference between surface and bulk passivation. In the first case, the ionic liquid [Ch][Cin] leads to the formation of particles on the perovskite surface [Figure 1(*b*),(*c*)]. The number of such particles increases with increasing IL concentration in isopropyl alcohol from 2.5 to 5 mM. XRD data include a weak reflection at 2θ of 10° [Figure 1(*f*)], indicating the appearance of an impurity phase as well. In the case of bulk passivation with 0.5–1% of [Ch][Cin], the perovskite films retain their initial smooth morphology [Figure 1(*d*),(*e*)]. According to XRD data, there is no visible difference between the diffraction patterns of the control sample and samples passivated by both methods, despite the small amount of impurity in the surface-passivated perovskite [Figure 1(*f*),(*g*)].

The nature of particles appearing on the surface of perovskite films after surface passivation with IL has been studied in detail. For this purpose, lead iodide and IL were mixed in equimolar quantities and the mixture was kept in methoxyethanol at a temperature of 60 °C with constant stirring for several days. The XRD pattern of the resulting powder shows the most intense diffraction peak at 10°, coinciding with the previously observed impurity reflection of surface passivated perovskite films [Figure 1(*f*)]. Interestingly, the same impurity is formed in bulk passivated films with a higher IL content of 5% [Figure 2(*a*)]. An analysis of the XRD pattern of the phase obtained from PbI_2 and [Ch][Cin] IL reveals that, presumably, this phase is heterogeneous PbI_2 with a larger distance between the layers where the choline cation could penetrate [Figure 2(*b*)].‡ Notably, the possibility of the formation of such a phase was also reported by Liu *et al.*[28]

According to steady-state PL data, surface passivation leads to a decrease in intensity and to a slight red shift of the emission line in the spectra of perovskite films (Figure 3). This indicates deterioration in optoelectronic properties and the possible formation of shallow defect states within the bandgap of perovskite films during surface passivation with IL. On the contrary, bulk passivation improves perovskite properties: 0.5% [Ch][Cin] leads to a 10% increase in PL intensity, while 1% IL promotes a blue shift of 3 nm. A concentration of 0.5% [Ch][Cin] appears to be optimal, which is typical for this

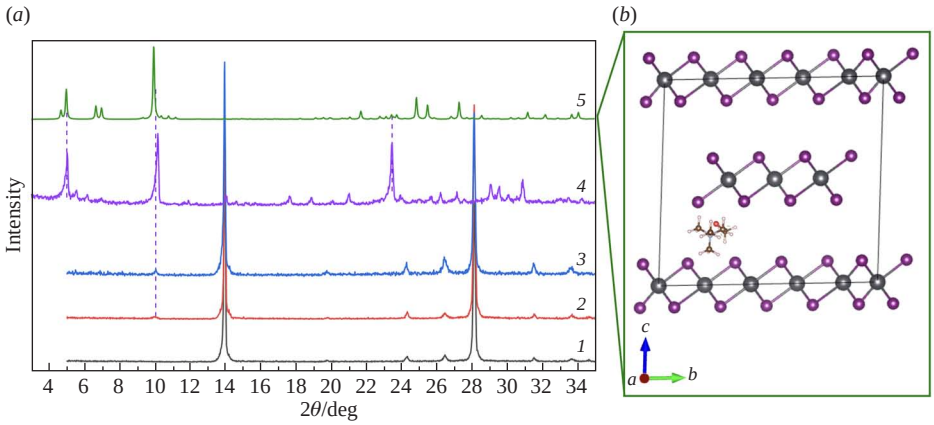

Figure 2 (*a*) Experimental XRD patterns of (*1*) a control perovskite film, (*2*) a film passivated on the surface with 5 mM IL, (*3*) a film passivated in bulk with 5% IL and (*4*) the reaction product of PbI_2 with IL, as well as (*5*) theoretical XRD pattern of the impurity phase formed in perovskite films, calculated using the lattice cell parameters of *(b)* the possible crystal structure shown.

the perovskite precursor solution. Surface passivation was performed by spin-coating a solution of ILs in isopropyl alcohol, followed by annealing the film at 100 °C for 5 min. All the samples were analyzed by scanning electron microscopy (SEM), X-ray diffraction (XRD) and steady-state photoluminescence spectroscopy (PL).

‡ *Crystal structure parameters of the impurity phase obtained from PbI_2 and [Ch][Cin] IL.* Crystal system: triclinic, space group *P*1, a = 9.861, b = 18.112 and c = 19.168 Å, α = 86.0°, β = 82.1°, γ = 79.8°, V = 3333.03 Å^3, 2θ range of 3–35°. The parameters were refined with *R*-factor = 14%.

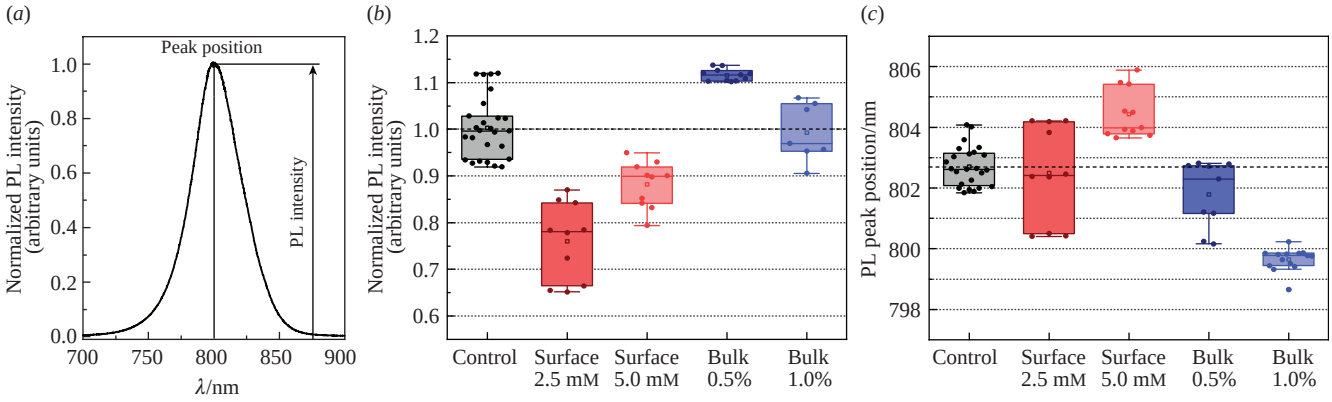

Figure 3 (*a*) Steady-state PL spectrum of a control perovskite film, indicating two parameters, peak intensity and peak position, which are used for statistical analysis of the PL properties of perovskite samples. Statistical distribution of (*b*) PL intensity (all normalized to the control sample) and (*c*) PL peak positions of the control sample and samples passivated using both methods.

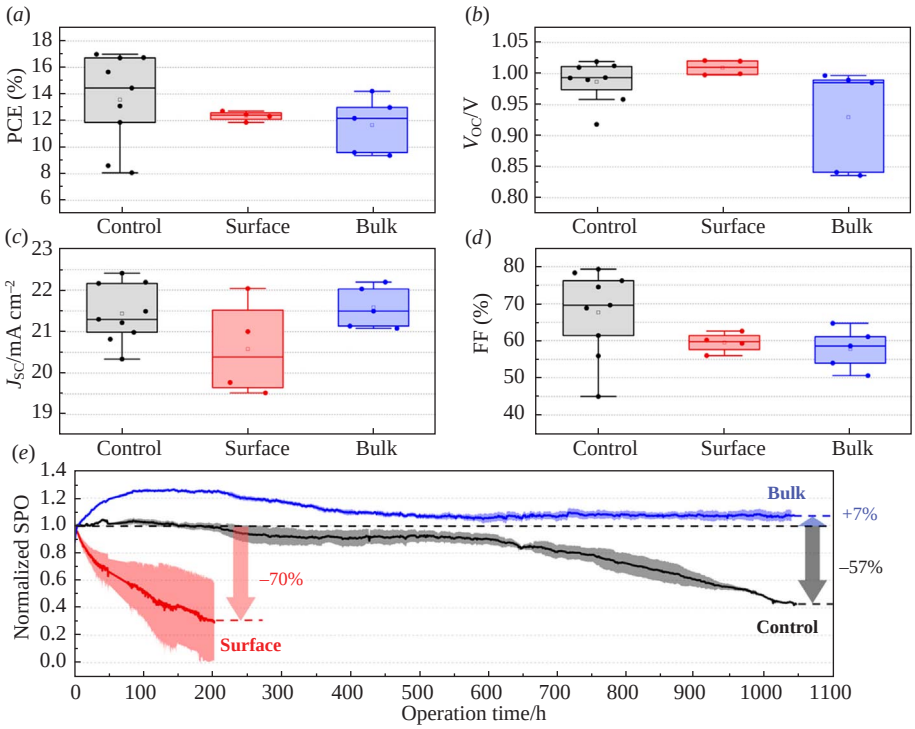

Figure 4 (*a*)–(*d*) *Operando* parameters of control PSCs (black) and PSCs with surface (2.5 mM IL, red) and bulk (0.5% IL, blue) passivation: (*a*) PCE, (*b*) V_{OC}, (*c*) J_{SC} and (*d*) FF. (*e*) Averaged stabilized power output (SPO) lines of encapsulated devices in MPPT regime under continuous 1 sun illumination at 55 °C in ambient air. The shadow areas around each curve show the distribution of efficiency values when examining two or more pixels for each device.

passivation method[29,30] and may be associated with deterioration in film crystallinity due to excess additive.

To investigate the effect of passivation with [Ch][Cin] on *operando* parameters and solar cell stability, PSCs with an inverted architecture were assembled.§ According to *J*–*V* measurements, passivation with [Ch][Cin] provides a small reduction in PCE from ~13.5% for the reference devices to ~12.3% and ~11.7% for surface and bulk passivation, respectively [Figure 4(*a*)]. The decrease in device efficiency upon surface passivation is associated with a loss of short-circuit current density (J_{sc}) and fill factor (FF), which indicates a loss of conductivity at the perovskite/electron-conducting layer interface [Figure 4(*c*),(*d*)]. This behavior probably originates from the appearance of an insulating impurity phase at the abovementioned interface, which reduces its conductivity. On the other hand, the decrease in PCE in bulk-passivated PSCs occurs mostly due to V_{oc} and FF losses, likely due to the appearance of defective states. Long-term photothermal stability testing of encapsulated solar cells was conducted under continuous 1 sun illumination at ~55 °C in ambient air in the continuous maximum power point tracking (MPPT)¶ regime.

§ Perovskite solar cells were assembled in the inverted p–i–n architecture of ITO/PTAA/MgF_2/perovskite/C_{60}/BCP/Cu/MgF_2. A layer of poly[bis(4-phenyl)(2,4,6-trimethylphenyl)amine] (PTAA) was spin-coated (5000 rpm, 30 s) from a 2 mg ml^{-1} solution in toluene (35 μl) onto a glass substrate with indium tin oxide (ITO) in an inert glovebox. After this, a layer of MgF_2 1 nm thick was deposited by thermal vacuum evaporation. Then, perovskite films were spin-coated from a 1.5 M solution in a DMF–DMSO mixture (4 : 1, v/v) and annealed at 125 °C for 60 min. Layers of C_{60}, bathocuproine (BCP), Cu electrode and MgF_2 (a protective layer for subsequent encapsulation) were successively deposited by thermal vacuum evaporation. The resulting solar cells were eventually encapsulated with a commercially available UV-curable polymer and a cover-glass slide as described previously.[9]

¶ *J*–*V* curves of the assembled devices were recorded under simulated AM 1.5G sunlight illumination with a power density of 100 mW cm^{-2} in quasi-steady-state mode (20 s per point) in the reverse scanning direction. Long-term photothermal stability testing of encapsulated PSCs in ambient air was carried out using an unfiltered LG PSH 0731B sulfur

MPPT data demonstrate that bulk passivation with 0.5% [Ch][Cin] results in an improvement in initial PCE within the first 150 h, surpassing the performance of the control device and achieving a PCE of nearly 16%. The overall stability of bulk-passivated devices improves markedly: after 950 h of simultaneous light soaking and heating, 107% of the initial PCE is retained [Figure 4(*e*), blue line], while control devices lose 45% of PCE. The surface passivation, on the contrary, leads to a significant loss of stability compared to the control devices [Figure 4(*e*), red line], which we attribute to the deterioration of the perovskite/C_{60} interface due to the growth of impurity particles.

As a result, we experimentally demonstrated the fundamental difference between the bulk and surface methods of perovskite passivation with the ionic liquid choline cinnamate. Bulk passivation with a preferred IL concentration of 0.5% makes it possible to improve the emission properties of the perovskite, retain good film morphology and significantly enhance the photothermal stability of PSCs. Surface passivation, in turn, leads to a deterioration in the emission properties of the perovskite, promotes the undesirable formation of a possibly dielectric impurity phase at the interfaces and ultimately leads to a strong decrease in the photothermal stability of PSCs.

This work was carried out with financial support from the Russian Science Foundation (grant no. 22-73-00286). XRD and SEM studies were performed using the equipment of the Joint Research Center for Physical Methods of Research of the Kurnakov Institute of General and Inorganic Chemistry of the Russian Academy of Sciences (JRC PMR IGIC RAS). The authors thank Anna V. Vavina, Marina M. Seitkalieva and Valentin P. Ananikov from the Zelinsky Institute of Organic Chemistry for providing the ionic liquid [Ch][Cin] for the experiments.

References

1 P. Čulík, K. Brooks, C. Momblona, M. Adams, S. Kinge, F. Maréchal, P. J. Dyson and M. K. Nazeeruddin, *ACS Energy Lett.*, 2022, **7**, 3039; https://doi.org/10.1021/acsenergylett.2c01728.
2 M. De Bastiani, V. Larini, R. Montecucco and G. Grancini, *Energy Environ. Sci.*, 2023, **16**, 421; https://doi.org/10.1039/d2ee03136a.
3 [dataset] NREL, *Best Research-Cell Efficiency Chart*, 2023; https://www.nrel.gov/pv/cell-efficiency.html.
4 Z. Song, A. Abate, S. C. Watthage, G. K. Liyanage, A. B. Phillips, U. Steiner, M. Graetzel and M. J. Heben, *Adv. Energy Mater.*, 2016, **6**, 1600846; https://doi.org/10.1002/aenm.201600846.
5 N. Aristidou, I. Sanchez-Molina, T. Chotchuangchutchaval, M. Brown, L. Martinez, T. Rath and S. A. Haque, *Angew. Chem., Int. Ed.*, 2015, **54**, 8208; https://doi.org/10.1002/anie.201503153.
6 F. Lang, O. Shargaieva, V. V. Brus, H. C. Neitzert, J. Rappich and N. H. Nickel, *Adv. Mater.*, 2018, **30**, 1702905; https://doi.org/10.1002/adma.201702905.
7 N.-K. Kim, Y. H. Min, S. Noh, E. Cho, G. Jeong, M. Joo, S.-W. Ahn, J. S. Lee, S. Kim, K. Ihm, H. Ahn, Y. Kang, H.-S. Lee and D. Kim, *Sci. Rep.*, 2017, **7**, 4645; https://doi.org/10.1038/s41598-017-04690-w.
8 N. N. Udalova, S. A. Fateev, E. M. Nemygina, A. Zanetta, G. Grancini, E. A. Goodilin and A. B. Tarasov, *ACS Appl. Mater. Interfaces*, 2022, **14**, 961; https://doi.org/10.1021/acsami.1c20043.
9 N. A. Belich, A. A. Petrov, P. A. Ivlev, N. N. Udalova, A. A. Pustovalova, E. A. Goodilin and A. B. Tarasov, *J. Energy Chem.*, 2023, **78**, 246; https://doi.org/10.1016/j.jechem.2022.12.010.
10 Z. Ni, H. Jiao, C. Fei, H. Gu, S. Xu, Z. Yu, G. Yang, Y. Deng, Q. Jiang, Y. Liu, Y. Yan and J. Huang, *Nat. Energy*, 2022, **7**, 65; https://doi.org/10.1038/s41560-021-00949-9.
11 J. Hieulle, A. Krishna, A. Boziki, J.-N. Audinot, M. U. Farooq, J. Ferreira Machado, M. Mladenović, H. Phirke, A. Singh, T. Wirtz, A. Tkatchenko, M. Graetzel, A. Hagfeldt and A. Redinger, *Energy Environ. Sci.*, 2024, **17**, 284; https://doi.org/10.1039/d3ee03511e.
12 Z. Zhang, L. Qiao, K. Meng, R. Long, G. Chen and P. Gao, *Chem. Soc. Rev.*, 2023, **52**, 163; https://doi.org/10.1039/d2cs00217e.
13 B. Chen, P. N. Rudd, S. Yang, Y. Yuan and J. Huang, *Chem. Soc. Rev.*, 2019, **48**, 3842; https://doi.org/10.1039/c8cs00853a.
14 R. Xia, Z. Fei, N. Drigo, F. D. Bobbink, Z. Huang, R. Jasiūnas, M. Franckevičius, V. Gulbinas, M. Mensi, X. Fang, C. Roldán-Carmona, M. K. Nazeeruddin and P. J. Dyson, *Adv. Funct. Mater.*, 2019, **29**, 1902021; https://doi.org/10.1002/adfm.201902021.
15 X. Zhu, M. Du, J. Feng, H. Wang, Z. Xu, L. Wang, S. Zuo, C. Wang, Z. Wang, C. Zhang, X. Ren, S. Priya, D. Yang and S. (F.) Liu, *Angew. Chem., Int. Ed.*, 2021, **60**, 4238; https://doi.org/10.1002/anie.202010987.
16 S. Bai, P. Da, C. Li, Z. Wang, Z. Yuan, F. Fu, M. Kawecki, X. Liu, N. Sakai, J. T.-W. Wang, S. Huettner, S. Buecheler, M. Fahlman, F. Gao and H. J. Snaith, *Nature*, 2019, **571**, 245; https://doi.org/10.1038/s41586-019-1357-2.
17 A. V. Vavina, M. M. Seitkalieva, A. V. Posvyatenko, E. G. Gordeev, E. N. Strukova, K. S. Egorova and V. P. Ananikov, *J. Mol. Liq.*, 2022, **352**, 118673; https://doi.org/10.1016/j.molliq.2022.118673.
18 A. Alashkar, M. Ayoub, T. Ibrahim, M. Khamis, P. Nancarrow, A. H. Alami and N. Tabet, *Int. J. Thermofluids*, 2023, **20**, 100404; https://doi.org/10.1016/j.ijft.2023.100404.
19 J. H. Lee, B. Nketia-Yawson, J.-J. Lee and J. W. Jo, *Chem. Eng. J.*, 2022, **446**, 137351; https://doi.org/10.1016/j.cej.2022.137351.
20 Z. Zhang, Z. Jiang, W. Ji, J. Fu, T. Wu, W. Wu, D. Rui, P. Xu, Y. Zhou, B. Dong and B. Song, *Adv. Energy Sustainability Res.*, 2023, **4**, 2200173; https://doi.org/10.1002/aesr.202200173.
21 S. Mariotti, D. Mantione, S. Almosni, M. Ivanović, T. Bessho, M. Furue, H. Segawa, G. Hadziioannou, E. Cloutet and T. Toupance, *J. Mater. Chem. C*, 2022, **10**, 16583; https://doi.org/10.1039/d2tc02633c.
22 J. Luo, F. Lin, J. Yuan, Z. Wan and C. Jia, *ACS Mater. Lett.*, 2022, **4**, 1684; https://doi.org/10.1021/acsmaterialslett.2c00091.
23 F. Wang, W. Geng, Y. Zhou, H.-H. Fang, C.-J. Tong, M. A. Loi, L.-M.Liu and N. Zhao, *Adv. Mater.*, 2016, **28**, 9986; https://doi.org/10.1002/adma.201603062.
24 Z. Wang, R. Li, M. Zhang and M. Guo, *Ceram. Int.*, 2022, **48**, 212; https://doi.org/10.1016/j.ceramint.2021.09.096.
25 Q. Sun, X. Meng, J. Deng, B. Shen, D. Hu, B. Kang and S. R. P. Silva, *J. Alloys Compd.*, 2023, **959**, 170478; https://doi.org/10.1016/j.jallcom.2023.170478.
26 X. Zheng, B. Chen, J. Dai, Y. Fang, Y. Bai, Y. Lin, H. Wei, X. C. Zeng and J. Huang, *Nat. Energy*, 2017, **2**, 17102; https://doi.org/10.1038/nenergy.2017.102.
27 G. Li, Z. Su, L. Canil, D. Hughes, M. H. Aldamasy, J. Dagar, S. Trofimov, L. Wang, W. Zuo, J. J. Jerónimo-Rendon, M. M. Byranvand, C. Wang, R. Zhu, Z. Zhang, F. Yang, G. Nasti, B. Naydenov, W. C. Tsoi, Z. Li, X. Gao, Z. Wang, Y. Jia, E. Unger, M. Saliba, M. Li and A. Abate, *Science*, 2023, **379**, 399; https://doi.org/10.1126/science.add7331.
28 Q. Liu, Z. Ma, Y. Li, G. Yan, D. Huang, S. Hou, W. Zhou, X. Wang, J. Ren, Y. Xiang, R. Ding, X. Yue, Z. Du, M. Zhang, W. Zhang, L. Duan, Y. Huang and Y. Mai, *Chem. Eng. J.*, 2022, **448**, 137676; https://doi.org/10.1016/j.cej.2022.137676.
29 N. N. Udalova, N. N. Chertorizhskiy, E. N. Nemygina, A. V. Trubnikov, A. V. Kurkin, E. A. Goodilin and A. B. Tarasov, *Mendeleev Commun.*, 2023, **33**, 679; https://doi.org/10.1016/j.mencom.2023.09.028.
30 N. N. Udalova, A. K. Moskalenko, N. A. Belich, P. A. Ivlev, A. S. Tutantsev, E. A. Goodilin and A. B. Tarasov, *Nanomaterials*, 2022, **12**, 4357; https://doi.org/10.3390/nano12244357.

plasma lamp calibrated using reference Si cells to a power density of 100 ± 10 mW cm^{-2}. Additionally, the distance of the PSCs from the sulfur plasma lamp was adjusted to achieve values of the PSC current density similar to those obtained under the conditions of the solar simulator. This step was necessary to minimize the impact of differences in the spectra of the sulfur plasma lamp and the solar simulator on the efficiency and stability of PSCs. The temperature of the samples during irradiation was about 55 °C. MPPT was performed using a standard perturb and observe algorithm, and the voltage was updated every 5 min in 10 mV increments using a homemade electronic board with 16-channel MPPT capability. All the devices were tested using a round metal aperture with an area of 9.348 mm^2 defined by a precision laser cutting.

Received: 2nd May 2024; Com. 24/7483